RESEARCH ARTICLE | DECEMBER 23 2024

Molecular dynamics studies of knotted polymers

Special Collection: Molecular Dynamics, Methods and Applications 60 Years after Rahman

Mark DelloStritto ; Cristian Micheletti ; Michael L. Klein

J. Chem. Phys. 161, 244904 (2024)
https://doi.org/10.1063/5.0237773
CHORUS

The Journal of Chemical Physics ARTICLE pubs.aip.org/aip/jcp

Molecular dynamics studies of knotted polymers

Cite as: J. Chem. Phys. 161, 244904 (2024); doi: 10.1063/5.0237773
Submitted: 6 September 2024 • Accepted: 4 December 2024 •
Published Online: 23 December 2024

Mark DelloStritto,[1,a)] Cristian Micheletti,[2] and Michael L. Klein[1]

AFFILIATIONS

[1] Institute for Computational Molecular Science, Temple University, Philadelphia, Pennsylvania 19122, USA
[2] International School for Advanced Studies (SISSA), I-34136 Trieste, Italy

Note: This paper is part of the JCP Special Topic on Molecular Dynamics, Methods and Applications 60 Years After Rahman.
[a)]**Author to whom correspondence should be addressed:** tuh39227@temple.edu

ABSTRACT

Molecular dynamics calculations have been used to explore the influence of knots on the strength of a polymer strand. In particular, the mechanism of breaking 3_1, 4_1, 5_1, and 5_2 prime knots has been studied using two very different models to represent the polymer: (1) the generic coarse-grained (CG) bead model of polymer physics and (2) a state-of-the-art machine learned atomistic neural network (NN) potential for polyethylene derived from electronic structure calculations. While there is a broad overall agreement between the results on the influence of the pulling rate on chain rupture based on the CG and atomistic NN models, for the simple 3_1 and 4_1 knots, significant differences are found for the more complex 5_1 and 5_2 knots. Notably, in the latter case, the NN model more frequently predicts that these knots can break not only at the crossings at the entrance/exit but also at one of the central crossing points. The relative smoothness of the CG potential energy surface also leads to stabilization of tighter knots compared to the more realistic NN model.

I. INTRODUCTION

The first computer simulation of an atomic liquid, which was carried out on the Mathematical Analyzer Numerical Integrator and Automatic Computer (MANIAC) at the Los Alamos National Laboratory, utilized a Monte Carlo algorithm to sample the relevant configuration phase space.[1] A few years later, Alder and Wainwright at the Lawrence Livermore National Laboratory reported the discovery of a phase transition in a system of hard spheres by carrying out molecular dynamics (MD) calculations.[2,3] In 1960, at the Brookhaven National Laboratory, Vineyard and co-workers reported molecular dynamics studies of radiation damage to crystals, caused by the impact of energetic particles.[4] In 1964, Rahman, while working at the Argonne National Laboratory, reported a molecular dynamics calculation for liquid argon.[5] As noted by Verlet in his speech at the September 1987 Rahman Memorial Meeting that was held at CECAM in Paris, "Anees was the first to 'simulate,' without any disguise or alibi, real bulk matter by integrating Newton's equation of motion." Notably, all these pioneering computational studies of condensed phases were carried out in the U.S. National Laboratories.

Not long after Rahman's pioneering molecular dynamics simulation of a "real" liquid, "Fast Computing Machines" began to appear in research universities, not only in the USA but also in Europe. Thereafter, molecular dynamics applications slowly began to proliferate. Indeed, during a sabbatical at Yeshiva University in 1967, Verlet used molecular dynamics to study the thermodynamic properties of the Lennard-Jones system.[6] Later, Verlet noted[7] that 280 years earlier, Newton's method for solving the equations of motion of celestial bodies[8] employed the same integration algorithm as the one that he had proposed and utilized for atoms.[9]

The invention of new algorithms and methodologies, plus the ever-expanding capabilities of computers over the past 60 years, has fueled an explosive growth in applications of molecular dynamics,[10–29,59] with innovations continuing to the present time.[30–33] Indeed, molecular dynamics is now an entrenched methodology/tool for studying diverse phenomena, such as melting and crystallization, wetting and de-wetting, glass formation, material transport and separations, molecular self-assembly, as well as the properties of materials as diverse as natural and synthetic macromolecules, plasmas, colloids, and active matter.

No field of science has escaped attention, with seminal contributions from molecular dynamics to contemporary research across a swath of disciplines, including biology, chemistry, physics, geology, planetary science, biochemistry, biophysics, neuroscience, physiology, and immunology, to name some of the currently active

application fields. Of course, molecular dynamics is not the only important tool to emerge from the birth of "Fast Computing Machines." Indeed, the fields of computer and information sciences owe their foundation, in no small measure, to pioneers from the dawn of the computer age: Turing[34] and John von Neumann.[35]

As a celebration of 60 years of molecular dynamics simulations, this article presents new results concerning the behavior of knots in macromolecules. In particular, our contribution compares and contrasts molecular dynamics results on knots using a traditional bead–spring polymer model[23] with molecular dynamics calculations on polyethylene (PE) with forces derived from machine-learned atomic potentials that have been fitted to electronic structure calculations on hydrocarbons obtained from state-of-the-art density functional theory (DFT).[28]

One of the central challenges in molecular dynamics is the creation of accurate interatomic potentials, and this has driven a large part of molecular dynamics research for several decades. The earliest potentials, such as the Lennard-Jones potential, included only non-bonded, spherically symmetric potentials, which, despite their utility in modeling certain materials, have severe limitations on their applicability. The introduction of bond, angle, and dihedral potentials greatly expanded the utility of molecular dynamics, allowing scientists to simulate the structure and dynamics of molecular systems.[36,37] The application of molecular dynamics to organic chemistry in particular has led to enormous advancements in our understanding of protein structure and function, the mechanism of action of pharmaceuticals at the molecular scale, and the development of new treatments and therapies.[38,39] However, these potentials are still limited by the fixed topology of the molecules, such that for many years, reactive chemistry remained firmly in the domain of the much more accurate and expensive density functional theory based MD.

The first attempt at a "reactive" force field came when Tersoff introduced bond-order dependent potentials, which made the potential energy of each atom dependent on its local environment.[40] The environment-dependent nature of the Tersoff potential allows simulating much more complex materials as the potential energy surface is allowed to vary along with the local symmetry of the material, mimicking the changes in the charge density observed when materials such as Si undergo a phase transition. These ideas were expanded upon to make the first truly reactive potential ReaxFF, which has been used to study proton transfer, combustion, and catalysis.[41,42] Despite its success, however, ReaxFF still faces two major challenges that have yet to be addressed: relatively simple non-bonded interactions and the fitting complexity. Regardless of the sophistication of the bonded interactions in ReaxFF, it can still be difficult for it to reproduce the structure and response of complex materials such as poly(p-phenylene terephthalamide) (PPTA), where H-bonds and aromatic ring interactions dominate intermolecular interactions.[43] This might be fixed with more complex non-bonded potentials; however, this will only contribute to the complexity of the fitting procedure, which can be prohibitively difficult and necessitates many versions of ReaxFF for different systems. These unresolved issues thus left much of materials modeling largely in the realm of DFT-MD and precluded the simulation of chemical reactions in disordered environments or as part of rare events.

The field of molecular dynamics was thus held back by twin problems: the need for complexity in the potential energy function and the difficulty of fitting such complex functions. These issues have mostly been solved by introducing machine learning and, in particular, neural networks (NNs) into potential energy functions. While it was first demonstrated that NNs could fit simple PESs for small molecules,[44,45] a breakthrough came when Behler and Parrinello demonstrated a generalized method to use a NN to fit potential energy surfaces as functions of the local symmetry around each atom.[28] While there have been many variations of this method since the first publication, the essential approach has largely remained unchanged. The main advantages of this method are (1) that no distinction is made between bonded and non-bonded interactions in the local symmetry and (2) that highly efficient and robust algorithms exist for optimizing the parameters of a NN.

Neural network potentials (NNPs) can thus be used to fit complex functions of the local symmetry up to a roughly 1 nm radius with relative ease. NNPs have led to incredible growth in our ability to simulate complex interactions in large systems, such as proton transfer at titania interfaces,[46] nanocrystalline metals,[47] and general models of combustion.[48] One can even couple these models with path integral molecular dynamics to study nuclear quantum effects.[49] Note, however, that even such sophisticated methods still lie within the Born–Oppenheimer approximation, such that further modifications are necessary to study, e.g., momentum transfer between electronic and nuclear coordinates.[50]

Here, we derive and apply NN potentials to study the effect of topological constraints in polymer systems and compare the findings with conventional molecular dynamics simulations of coarse-grained (CG) polymer models. Intra- and inter-chain topological entanglements, such as knots, are ubiquitous in systems with sufficiently long and densely packed polymers and can profoundly impact their physical properties.[51] For instance, equilibrated polymer melts evolve slowly because the primary relaxation mode available to the chain is the reptation along the one-dimensional tube established by inter-chain entanglements.[52] Adding mechanical stress or applying shear through elongational flows and external fields can further hinder the dynamics[53–58] by tightening the interlockings and, therefore, suppressing fluctuations. These consequences of topological entanglements have mainly been studied with a focus on the numerosity or density of chain interlocking and, therefore, the role of the complexity and degree of localization of the interlockings is much less understood.

Motivated by these considerations, we used NN potentials to study, in atomistic detail, how individual knotted polymer chains respond to the application of increasing mechanical stress. We analyzed and compared the response of chains with 3_1, 4_1, 5_1, and 5_2 knots, hence covering different knot families and complexities. The setup allowed us to reveal multiple modes for how strain can accumulate along the knot contour, providing a mechanistic rationale for the observed free-energy barriers to bond rupture as well as topological friction. Finally, by comparing the findings with those obtained for a coarse-grained polymer model, we offer the first characterization of the interplay of chain topology and microscopic structural details, showing that the latter can modify both qualitatively and quantitatively how the chain responds to applied tensile stress.

II. METHODS

All DFT calculations were run with the plane-wave module of Quantum Espresso (v.7.0)[59,60] using the r^{2}SCAN meta-GGA functional,[61] a plane-wave cutoff of 240 Ry, SCAN Troullier–Martins norm-conserving pseudopotentials,[62] and a Monkhorst–Pack reciprocal grid with a spacing of ~0.2 Å^{-1}. Most structures were assumed to have zero spin; however, in those cases where bonds have been broken or atoms removed, such that the system contains radical end groups or unpaired electrons, we assumed an antiferromagnetic spin configuration.

A comprehensive set of training structures was created across many possible hydrocarbon structures. We included structures of small alkanes, alkenes, alkynes, alkadienes, alkatrienes, and aromatic hydrocarbons, including crystal structures when available, in addition to random packings achieved with PACKMOL.[63] Structures of polyethylene in the orthorhombic and hexagonal phases were added, as well as disordered liquid decane structures as an approximation of disordered PE. We included spin defects in the training set, including a decane molecule with two H atoms removed from either end, butylene defects in PE, and broken PE chains with radical end groups. During the training process, we simulated a PE knot with a NNP and then added those structures back into the training set, including both whole and broken PE knots.

The NNP is defined by 16 radial symmetry functions and 8 angular symmetry functions, with a cutoff of 6 Å. The neural network has three layers with 28 nodes per layer. The radial symmetry functions are defined using the log-cosh function and a cosine cutoff function,[64] forming a radial basis that smoothly transitions from functions with wide support and small gradients to functions with narrow support and large gradients at short distances. The angular symmetry functions are the G4 angular symmetry functions introduced by Behler.[64]

A. Atomistic simulations

The simulations were started from the idealized open knot structures shown in Fig. 1(a), corresponding to the 3_1, 4_1, 5_1, and 5_2 prime knots, and consist of 100 equispaced beads. Each bead was mapped to a C atom, and the corresponding H atoms were subsequently assigned. The resulting knotted polyethylene chains were then initially equilibrated and tightened slightly using the Optimized Potentials for Liquid Simulations-All Atom (OPLS-AA) potential.[65] Typical configurations at the end of these steps are shown in Fig. 1(b). The temperature was held constant at 300 K using a Langevin thermostat with a unique initialization of the velocities for each simulation, and the time step used was 0.25 fs. In the production run, the relaxed configurations were stretched by pulling the two ends in opposite directions with a force f, which increased linearly with time t as $f = r \cdot t$, where r is the loading rate.

B. Coarse-grained models and simulations

For the coarse-grained polymer, we considered a chain of 100 beads.

The excluded-volume interaction of any pairs of non-consecutive chain monomers (beads) was treated with a Weeks–Chandler–Andersen (WCA) potential, i.e., a truncated and shifted Lennard-Jones potential,

$$U_{\mathrm{WCA}} = \begin{cases} 4\epsilon\left[\left(\frac{\sigma}{r}\right)^{12} - \left(\frac{\sigma}{r}\right)^{6}\right] + \epsilon & \text{if } r \le \sqrt[6]{2}\sigma, \\ 0, & \text{otherwise,} \end{cases} \tag{1}$$

where the characteristic energy ϵ and the nominal bead diameter σ were used as the energy and length units, respectively.

The backbone connectivity was provided by a Morse potential acting between consecutive beads,

$$U_{\mathrm{Morse}} = D\left(1 - e^{-\alpha(r-\sigma)}\right)^2, \tag{2}$$

with $\alpha = 10\sigma^{-1}$ and $D = 100\epsilon$.

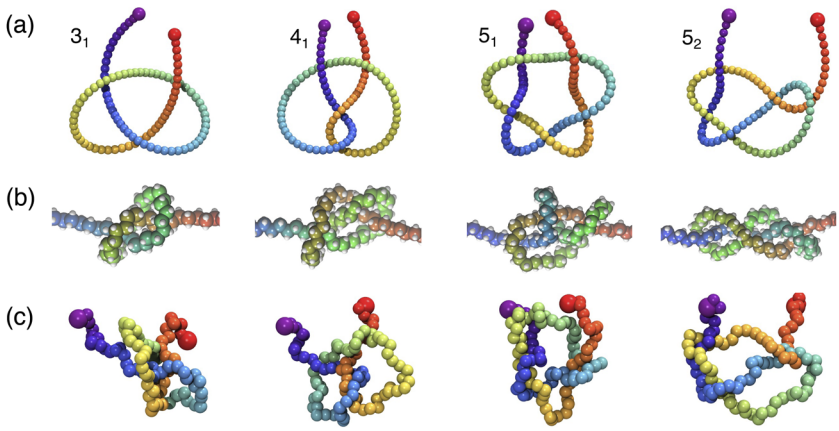

FIG. 1. (a) Idealized configurations of open knots used as initial templates for the atomistic simulations of polyethylene and for those of the coarse-grained polymer model. The closed version of these configurations corresponds to the four simplest types of non-trivial prime knots, i.e., 3_1, 4_1, 5_1, and 5_2 topologies. Relaxing and preconditioning the template conformations, see Sec. II, provided the initial states of the atomistic and coarse-grained force-ramping simulations, shown in panels (b) and (c), respectively. For clarity, monomers are sequentially colored with a rainbow scheme, and only the neighborhood of the knotted region is shown for the polyethylene chain.

The evolution of the system was studied using overdamped Langevin molecular dynamics simulations, with the temperature set by $k_BT = \epsilon$ and a unitary friction coefficient γ. The time step used was $0.005\tau_{MD}$, where $\tau_{MD} = 2\gamma/(D\alpha^2)$ is the characteristic simulation time.

The simulations were carried out in two stages. First, the idealized open knotted chains were freely evolved for $2.5 \times 10^4 \tau_{MD}$, sufficient for equilibration without spontaneous unknotting. Typical conformations at the end of this relaxation phase are shown in Fig. 1(c). In the subsequent production run, the two ends of relaxed configurations were pulled in opposite directions by a force f, which increased linearly with time t as $f = r \cdot t$, where r is the loading rate.

III. RESULTS AND DISCUSSION

Knots are statistically inevitable in equilibrated flexible polymers[66] and can have notable implications for the physical properties of such systems. For instance, constraining the conformational space of polymers to a specific knot type significantly biases the metric properties with respect to the topological unrestricted ensemble. The biases can make metric scaling deviate from the conventional one[67,68] while also allowing sorting of torsionally relaxed DNA rings by knot type by driving them electrophoretically through a gel mesh.[69,70] Dynamic properties can be notably affected, too. On the one hand, because knots reduce the effective chain contour length,[71–74] the Rouse relaxation modes of isolated entangled chains are typically faster than unknotted ones.[75] On the other hand, the lifetime of knots typically exceeds the Rouse time and, therefore, topological entanglement can introduce new and relevant characteristic relaxation timescales.[73] Such unusually slow relaxation modes have been observed in single molecule experiments on DNA filaments in spatial confinement,[76–78] a setting conducive to spontaneous knotting.[51,74,79–82]

Arguably, knots have their most noticeable impact on the mechanical properties of polymers and biopolymers. For example, DNA is a biopolymer long enough to form knots, and they can significantly hinder transcription[83–89] and translocation through pores.[90,91] Knots should also be common in long polymers, such as ultra-high molecular weight polyethylene[92] (UHMWPE), with an uknotting time in a melt that is a power law of the relative size of the knot compared to the total strand.[93] Such knots significantly weaken the strength of the polymer strand[93] and need to be avoided in bulk materials, but entanglements on a surface can enhance the binding between materials through friction between entangled chains.[94] This topological friction[95] manifests differently across the various knot topologies as the spatial distribution of the strain hotspots depends on the knot geometry.[96] Based on these premises, it is natural to hypothesize that the strain that accumulates in the tightened knotted region may crucially depend on the structural details of the polymer. Accordingly, general coarse-grained polymer models based on "smooth" structural representations, such as chains of beads, may be apt for revealing strain response patterns that vary across different families of knots, such as torus and twist ones,[96] but may possibly miss emergent features defined by the tight packing of the chemical groups of the polymer backbone or the monomeric units. To our knowledge, this problem has so far remained virtually unexplored.

Motivated by these considerations, here we use atomistic models of polyethylene and coarse-grained chains of beads to study how different knots affect the accumulation of strain and, eventually, the rupture of the filaments when they are pulled at both ends by an increasing stretching force. This setup, inspired by force-spectroscopy experiments, is arguably the simplest context in which to study the mechanics of tight knots because the load is applied symmetrically at both ends, unlike in pore translocation.

We considered the open knots shown in Fig. 1 corresponding to the four simplest non-trivial topologies: 3_1, 4_1, 5_1, and 5_2 knots. The labeling is based on the standard x_y nomenclature for (closed) knots, where x is the crossing number, i.e., the number of crossings in the simplest two-dimensional knot projection, and y is a conventional enumerative index.

The set includes prime knots with different nominal complexities, as indicated by the crossing number, belonging to different knot families. In particular, 3_1 and 5_1 are torus knots, while 3_1, 4_1, and 5_2 are twist knots (the 3_1 or the trefoil knot being a special case, belonging to both families).

A. Force-ramping protocol

As customary in force spectroscopy studies, we used a force-ramping approach to study the breaking of knotted polyethylene

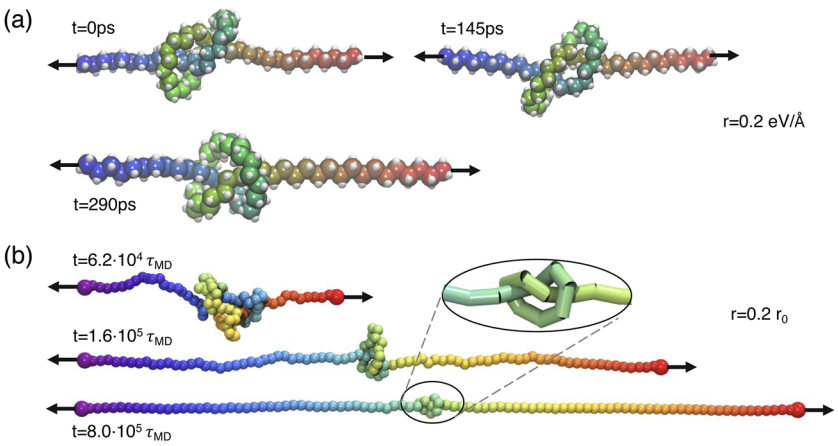

FIG. 2. Typical configurations of trefoil-knotted (a) polyethylene and (b) coarse-grained chains at the initial, intermediate, and final (pre-rupture) stages of the force-ramped stretching. The times and loading rates are indicated. For clarity, monomers are sequentially colored with a rainbow scheme, and only the neighborhood of the knotted region is shown for the polyethylene chain. The pulling rate of the coarse-grained model is expressed in terms of $r_0 = 2 \cdot 10^{-4}\epsilon/(\sigma\,\tau_{MD})$.

chains and contrasted it with the reference case of fully flexible chains of beads.

The two termini of the polymer chain were pulled in opposite directions by a force whose magnitude, f, was increased linearly with time at a rate r. Figure 2 illustrates typical configurations of the atomistic and coarse-grained trefoil knotted polymers at different stages of the process.

Independent force-ramping simulations were carried out starting from initially equilibrated conformations, which eventually disconnected under the increased load. We used 10–15 simulations for the atomistic NN model, while for the CG model, which is more computationally amenable, we typically used 200. For each trajectory, we recorded where exactly in the chain the failure occurred and at which force. The most probable rupture force f^* at a given loading rate was obtained from an optimal-bandwidth Gaussian kernel density analysis.[97] The most probable rupture forces for the atomistic NNP and CG knotted chains are plotted against the log of the loading rate in Fig. 3.

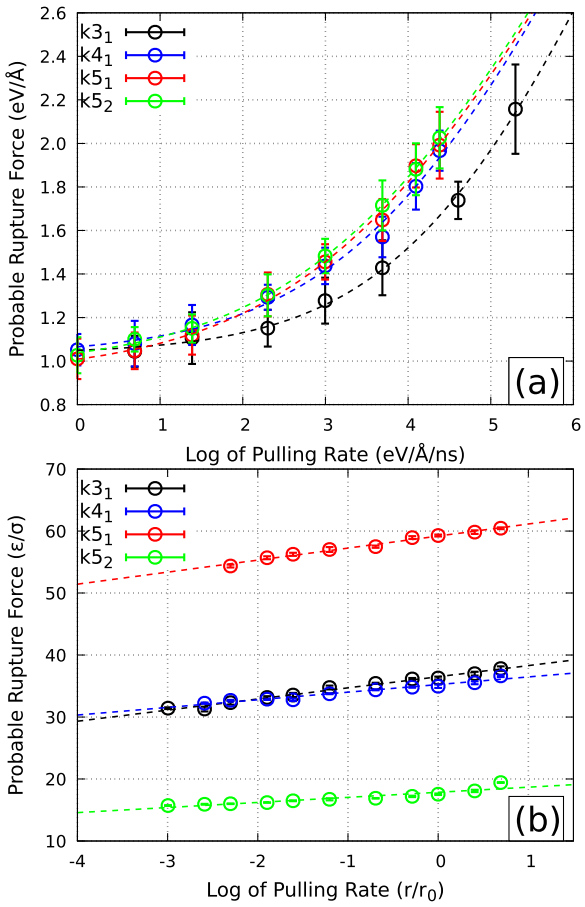

FIG. 3. Plot of the most probable rupture force as a function of the logarithm of the pulling rate for each knot simulated with (a) the atomistic NN model and (b) the coarse-grained model. The bars represent the statistical error on the most probable rupture force, determined via a Gaussian kernel density analysis. The dashed lines are best fits of the semi-log data obtained using a softplus function for the atomistic model and a linear function for the coarse-grained one.

The chain rupture response of the two models is significantly different. At fixed r, the most probable rupture force of the NNP polyethylene chains increases monotonically with the crossing number, with what appears to be a logarithmically increasing difference between knots with complexity, such that there is a large gap between the 3_1 and 4_1 barriers but much less of a difference between the 5_1 and 5_2 knots. By contrast, no such monotonicity is seen for the CG model, where f^* has a threefold variation across different knot types. Interestingly, the extreme rupture forces are systematically observed for the five-crossing knots, the lowest and highest f^* values corresponding to the twist (5_2) and torus (5_1) knots.

B. Bell–Evans–Polanyi analysis

To further interpret the data, we resorted to the Bell–Evans–Polanyi (BEP) analysis, which is commonly used to study the rupture of intra- and inter-molecular bonds in force-spectroscopy setups. The BEP theoretical framework is applicable when the activation barrier for the irreversible process (e.g., bond rupture) is sharp, meaning that the transition state is not significantly displaced by the application of the external force. This simplifying assumption allows deriving a closed expression for the most probable rupture force,[98–100]

$$f^* = \frac{K_B T}{\Delta} \cdot \ln\left(\frac{r \cdot \Delta}{\nu \cdot K_B T}\right) + \frac{E_T}{\Delta}, \tag{3}$$

where E_T and Δ are, respectively, the height and width of the barrier associated with the rupture event, ν is a kinetic coefficient, and r is the loading rate.

The best fits of the NNP and CG data obtained using the BEP functional form of Eq. (3) are illustrated by the dashed lines in Fig. 3. In the semi-log scale of the graph, the best fit procedure amounts to a linear interpolation of the data points. This is violated in the NNP at low pulling rates as each knot converges to the same rupture force, which we interpret as the minimum force required to break a single bond. From the viewpoint of Kramers' theory, this is due to "rebinding," where the unbound state is far above the bound state, and returning to the bound state is common.[98] Once we pass this regime, the trend becomes linear, and so we fit the NNP results using a softplus function.[101] We note that the slope of each line is largely the same in both models, which, from Eq. (3), indicates that the width of the barrier for the rupture of the chain is similar across the different knot types.

However, the two models differ significantly with regard to the range of y axis intercepts. Taking into account the similar slope of the lines is informative of the different heights of the barriers. The largest variation is seen for the CG model, with the smallest and highest barriers corresponding to the 5_2 (twist) and 5_1 (torus) knots. This large difference is intriguing considering that the two knots have the same nominal complexity. By contrast, the 3_1 (torus) and 4_1 (twist) knots have very similar energy barriers, despite their different crossing numbers. The NNP, on the other hand, yields BEP plots that monotonically increase with the complexity of the knot but only by a few hundredths of an eV/Å.

The above-mentioned results establish two main points: first, the fact that the breaking response depends on the knot type for

both models is a strong indication that the chain rupture directly involves the knotted region, and second, the rupture mechanism of knotted chains differs profoundly between the atomistic NN model of polyethylene and the coarse-grained model of fully flexible chains of beads. The two observations suggest that the starkly different rupture responses of the two panels in Fig. 3 are a reverberation of systematic and significant differences in the structural organization of the knotted regions in the two polymer models.

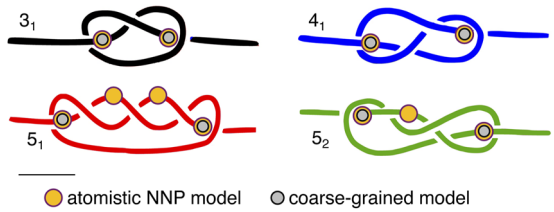

FIG. 4. Sketches of the typical rupture points observed in atomistic and coarse-grained models.

C. Rupture points analysis

To clarify the structural bases of the different knot rupture mechanisms in the atomistic NNP and CG models, we first analyzed where exactly the chains broke. For reference, we recall that the expected behavior for simple knots is that the rupture will occur at the entrance/exit of the knot, a result that has been demonstrated several times for both microscopic and macroscopic knots.[102–106]

The analysis of the trajectories revealed that the two simplest knot types, 3_1 and 4_1, indeed, break at the entrance/exit of the knotted region in both the atomistic and coarse-grained models, as shown in Fig. 4. In particular, for the intermediate loading rate of the CG model, $r = 0.3r_0$, the rupture occurred within two monomers of the knot boundaries in 192 of the 200 runs. The knot boundaries were detected using the KymoKnot software package,[107] which identifies the knotted region as the shortest chain portion that has a non-trivial topology once closed with a "minimally invasive" auxiliary arc.[108] We note that under sufficient tensile load, the initial twist geometry of the 4_1-knotted chain [Fig. 1(a)] is superseded by a figure-of-eight geometry [Figs. 1(b) and 4]. In this geometry, tight loops encircle the segments at the entrance and exit of the knot, not unlike the 3_1 knotted case. We conclude that the reason why the 3_1 and 4_1 knots have such similar barriers in Fig. 3(b), irrespective of the NN and CG models, is that the contact points that prime the rupture of the chain are similar in the two types of knots.

Consistent with the above-mentioned reasoning, the different barriers of the 5_1 and 5_2 knots in the CG and NNP chains are likewise reflected by the different positioning of the breaking points inside the knot. While in the fully flexible CG chain, the breaking points are concentrated only at the entrance and exit of the knotted region, in the atomistic NNP chains, they are frequently located in the interior. These additional points correspond to tightly hooked segments, with the rupture mostly occurring in correspondence with the most exposed segment of the two. The large variation in the barrier for breaking 5_1 and 5_2 knots in the CG model [Fig. 5(b)] can be rationalized considering the flexibility of this model polymer, which, unlike polyethylene, has no bending rigidity. Indeed, knots in the CG model can be pulled much more tightly than those in the NNP case: for intermediate loading rates, the pre-rupture average number of monomers spanned by the 3_1, 4_1, 5_1, and 5_2-knotted regions are 9.6, 13.5, 17.2, and 17.5 for the CG model and 32, 46, 54, and 54 for the NN model, respectively. Because knots are tighter, the different

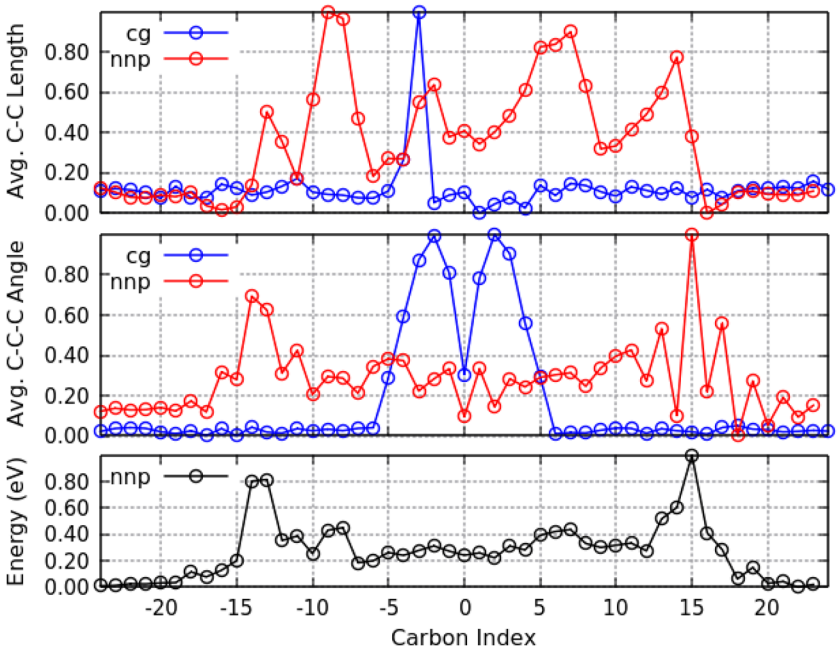

FIG. 5. Plot of the average C–C bond length and C–C–C angle averaged over a simulation of the 3_1 knot held at its length right before rupture for both the NN and CG potentials. In addition, the energy of each C atom yielded by the atomistic NNP is plotted. In order to compare the different values, the plots are centered at the center of the knot, and the values are centered by the mean and scaled by the minimum/maximum difference.

geometries of the contact regions of various knots become more evident and, hence, consequential for the chain rupture. In particular, the entrance and exit segments of 5_2 knots are even more encircled by (clasped) tight loops than for the 3_1 and 4_1 cases, while the opposite is true for the 5_1 case. These different features account for the observed hierarchy of tensile strengths shown in Fig. 5(b).

D. Structural analysis

The above-mentioned considerations prompted us to examine quantitatively the main geometric features that define the breaking points, namely the backbone bond lengths and bending angles.

For the coarse-grained models, these quantities are naturally defined by the length of the distance vector of two consecutive monomers and the angle formed by two such consecutive vectors or, equivalently, by a triplet of consecutive monomers. For the atomistic NN model, we, instead, considered the C–C bond lengths and the C–C–C angles. We calculated the bond and angle profiles individually for each run, averaging over the short time interval that preceded bond rupture. For the CG model, this means ten frames before rupture, while for the NN model, we simulated the knot at a fixed length for 10 ps before rupture for 40 ps in order to reduce the noise of the averages.

Figure 5 presents typical instances of bond and angle profiles in atomistic and CG chains. To facilitate comparison, each profile was linearly rescaled by mapping the minimum and maximum values to 0 and 1, respectively. In addition, the monomer index was shifted so that the knot midpoint corresponds to the origin of the x axis. The profiles shown in Fig. 5 correspond to the 3_1 knot case; equivalent figures for the other considered knot types are provided in the supplementary material.

The atomistic and CG profiles in Fig. 5 present several noticeable differences. The first notable element is the different breadths of the regions, where the profiles deviate from the baseline level. These are a direct manifestation of the different contour lengths of the knotted regions prior to rupture. For 3_1 knots, such regions involve, on average, 32 and 16 monomers for the NN and CG models, respectively. Note that the region where the angle profiles differ from the baseline level slightly extends beyond the knot. This is because the strain of hooked strands in the tightly pulled knots causes the chain backbone to bend in proximity to the knot entrance and exit points (see Fig. 2).

In addition, the CG model profile presents two smooth, pronounced peaks that are specular with respect to the knot midpoint, while the atomistic one is more fluctuating, and the peaks are neither symmetric nor equally high. In both cases, the highest (peak) curvatures are found in correspondence to the loops that constrict the strands entering and exiting the knot. Instead, the midpoint of the arc that bridges these two loops is a local minimum of curvature and corresponds to the center of the knot.

Further differences emerge from the comparison of the bond length profiles. The CG one presents a single peak located in correspondence with the bond that would eventually rupture in the considered run. The sharpness of the peak reveals that this bond is virtually the only one that is distorted by the accumulated strain. The strained bond is one of the two bonds that are constricted by the high-curvature loops, consistent with the typical location of the rupture points shown in Fig. 4.

Instead, the bond length profile of the atomistic NN model presents two peaks in correspondence with the knot entrance and exit points and three more peaks inside the knotted region. Overall, there are five distinct regions with strained bonds. This multimodality of the strain profile has no analog in the CG case and is an emergent feature of the atomistic NN model, given that it is systematically observed for all considered knot types (see the supplementary material).

Based on the structural analysis, we conclude that the mechanisms leading to the rupture of topologically constrained chains are qualitatively different for the atomistic and CG polymer models. In the latter, the systematic breaking points of the chains are limited to the entrance and exit points of the knot, where the backbone is constricted by tight and, hence, highly curved loops. Instead, the tight knots in the atomistic model span many more monomers and present more varied profiles for bond lengths and angles so that the breaking points cannot be determined as straightforwardly from the sole inspection of the local geometric observables.

E. Analysis of energy profile

To gain more insight into the more complex behavior of the NNP chains, we extended considerations to the potential energy for each C atom (see the bottom panel of Fig. 5).

The energy profile is more regular than the bond length and angle ones, featuring only two peaks observed in correspondence with the knot boundaries. By computing the Pearson's correlation coefficient, we obtained the coefficient of determination for the energy with respect to the bond, angle, and the harmonic mean of the bond and angle. The data shown in Table I indicate that the energy is more strongly correlated with the angle than with the bond length and that the correlation is strongest for the mean of the two observables. This is consistent with previous detailed investigations of the dependence of the C energy on the C–C bond and C–C–C angle of 3_1 knots, where it was shown that the energy increased the most when the bond and angle increased simultaneously.[109] The energy profile thus clarifies that even though the bond and angle strains vary appreciably along the knot region, stress concentrates at the entrance and exit points of the knot, where chain breaks occur.

Although the typical 3_1-knot rupture points are the same for NNP and CG chains, the above-mentioned analysis and the data for the other knot types provided in the supplementary material indicate that the two polymer models are different in two important respects. On the one hand, the more complex structure and interactions of the monomers create more points of self-contact in the knotted region, with significant bond and angle strains. On the other hand, they prevent knots from tightening as much as in CG chains.

TABLE I. Coefficient of determination for the average C bond, angle, and the harmonic mean of the two with respect to the C energy.

Abscissa	R^2
Bond	0.137
Angle	0.569
Mean	0.643

The first aspect directly reflects on the more numerous points where chain breaks can occur in atomistic NNP chains compared to CG ones. The second aspect helps rationalize why the BEP curves of Fig. 3 appear to have a universal quality, i.e., they are less dependent on the specific knot type than CG chains. Because pre-rupture knots in CG chains span one-third or less of the monomers of NNP ones, the local geometrical features vary more conspicuously across the different knot types, including the curvature at the entrance and exit points. This is reflected in the enhanced differences of energy barriers observed in Fig. 3(b).

IV. CONCLUSIONS

Here, we harness an atomistic NNP to study a challenging problem in polymer physics, namely how knotted polyethylene chains rupture under increasing tensile load. These potentials allow unprecedented accuracy and insight into chemical reactions with much greater efficiency than quantum chemistry methods. We contrast the observed behavior with a coarse-grained chain of beads, as these CG models are a standard approach for studying large, disordered systems at long time scales. We addressed two main aspects of the problem: (i) the effect of topological complexity on the energy barriers to chain rupture and (ii) the mechanisms leading to the accumulation of strain and stress along the chain prior to the rupture event.

To this end, we considered the four simplest types of prime knots: 3_1, 4_1, 5_1, and 5_2, and for each topology, we carried out force-ramped simulations for a broad range of loading rates. The energy barriers were studied with a Bell–Evans–Polanyi analysis of the rupture forces, while for the strain and stress accumulation, we profiled structural and energy-related observables.

Our analysis revealed significant differences in the two polymer models. The energy barriers of the atomistic system, which was based on an atomistic NNP description of polyethylene, had similar heights and widths across the various knot types. By contrast, the coarse-grained system, which consisted of fully flexible chains of beads, presented very noticeable differences in barrier heights. In addition, the latter did not present a simple dependence on knot complexity. In fact, the two most complex knots accounted for the highest and lowest barriers, corresponding to the 5_1 torus knot and the 5_2 twist one.

Inspection of the trajectories revealed further differences regarding the location of the rupture points. For both models, these occurred in the knotted region. However, while in the coarse-grained case, the chain breaks almost exclusively involving the bonds at the knots' entrance and exit points, in the atomistic case, the rupture of the five-crossing knots frequently occurs in the interior of the knot as well. A detailed analysis of the chain backbone prior to rupture clarified that the more complex structure and interactions of the monomers of the atomistic model create several points of self-contact in the knotted region. The points are more numerous than for coarse-grained chains and, since they accumulate bond and angle strain, offer additional opportunities for chain breaks to occur. At the same time, the inherent finite bending rigidity of the atomistic chains is responsible for preventing the knotted region from becoming as tight as in the fully flexible chains of beads. As a consequence, the bending energy is more evenly distributed in the atomistic model. In this way, the local curvature profile of tight (pre-rupture) conformations of different knot types is more similar in the atomistic case than in the coarse-grained case, explaining the more similar energy barriers.

In conclusion, our study provides a first systematic comparison of topological friction and its mechanical implications in atomistic and coarse-grained polymer models. Our results have several implications. First, the stark qualitative differences observed for the mechanical resistance of knotted chains prove that varying the structural details of the chains can be just as consequential for their physical properties as varying the type of topological constraints. Second, the properties observed here ought to be transferable to other single-molecule setups, such as pore translocation, where mechanical tension is applied at one end of the chain, rather than two.[95,96] Finally, the current results stimulate the investigation of the effect of topological constraints in more general systems, such as melts of chains under strain, the impact of topological defects on the mechanical performance of polymer materials, and the impact of atomic-scale friction on polymer dynamics.

SUPPLEMENTARY MATERIAL

The supplementary material encompasses plots of the average bond, angle, and energy of each C atom for the 4_1, 5_1, and 5_2 knots computed using the atomistic NNP and typical conformations of knotted coarse-grained chains just before the rupture event.

ACKNOWLEDGMENTS

The contributions from M.L.K. and M.D. were supported in part by the U.S. Army Research Laboratory under Contract No. W911NF-21-2-0007. They are also grateful for partial support from the Computational Chemical Sciences Center: Chemistry in Solution and at Interfaces (CSI), which is funded under DOE Award No. DE-SC0019394. Invaluable high performance computing resources were provided by the U.S. National Science Foundation via Major Research Infrastructure Grant No. 1625061. C.M. acknowledges support from the European Union - NextGenerationEU, in the framework of the PRIN Project "The Physics of Chromosome Folding" (code: 2022R8YXMR, Grant No. CUP: G53D23000820006) and by PNRR Mission 4, Component 2, Investment 1.4_CN_00000013_CN-HPC: National Center for HPC, Big Data and Quantum Computing - spoke 7 (Grant No. CUP: G93C22000600001). The views and opinions expressed are solely those of the authors and do not necessarily reflect those of the European Union, nor can the European Union be held responsible for them.

AUTHOR DECLARATIONS

Conflict of Interest

The authors have no conflicts to disclose.

Author Contributions

Mark DelloStritto: Conceptualization (equal); Investigation (equal); Methodology (equal); Software (equal); Visualization

(equal); Writing – original draft (equal); Writing – review & editing (equal). **Cristian Micheletti**: Conceptualization (equal); Investigation (equal); Methodology (equal); Visualization (equal); Writing – original draft (equal); Writing – review & editing (equal). **Michael L. Klein**: Conceptualization (equal); Supervision (lead); Writing – review & editing (equal).

DATA AVAILABILITY

The data that support the findings of this study are available from the corresponding author upon reasonable request.

REFERENCES

[1]N. Metropolis, A. W. Rosenbluth, M. N. Rosenbluth, A. H. Teller, and E. Teller, "Equation of state calculations by fast computing machines," J. Chem. Phys. **21**, 1087–1092 (1953).

[2]B. J. Alder and T. E. Wainwright, "Phase transition for a hard sphere system," J. Chem. Phys. **27**, 1208–1209 (1957).

[3]B. J. Alder and T. E. Wainwright, "Studies in molecular dynamics. I. General method," J. Chem. Phys. **31**, 459–466 (1959).

[4]J. B. Gibson, A. N. Goland, M. Milgram, and G. H. Vineyard, "Dynamics of radiation damage," Phys. Rev. **120**, 1229 (1960).

[5]A. Rahman, "Correlations in the motion of atoms in liquid argon," Phys. Rev. **136**, A405 (1964).

[6]L. Verlet, *Chimères et paradoxes: comment penser le monde où nous vivons?* (Editions du Cerf, Paris, 2007).

[7]L. Verlet, "Computer 'experiments' on classical fluids. I. Thermodynamical properties of Lennard-Jones molecules," Phys. Rev. **159**, 98 (1967).

[8]I. Newton, *Philosophiae Naturalis Principia Mathematica* (Jussu Societatis Regiae ac Typis Josephi Streater. Prostat Venales apud Sam. Smith ad insigna Principis Walliae in Coemiterio D. Pauli, aliosq, nonnullos Bibliopolas, 1687).

[9]D. Levesque and J. P. Hansen, "The origin of computational statistical mechanics in France," Eur. Phys. J. H **44**, 37–46 (2019).

[10]J.-P. Ryckaert, G. Ciccotti, and H. J. C. Berendsen, "Numerical integration of the cartesian equations of motion of a system with constraints: Molecular dynamics of *n*-alkanes," J. Comput. Phys. **23**, 327–341 (1977).

[11]H. C. Andersen, "Molecular dynamics simulations at constant pressure and/or temperature," J. Chem. Phys. **72**, 2384–2393 (1980).

[12]M. Parrinello and A. Rahman, "Crystal structure and pair potentials: A molecular-dynamics study," Phys. Rev. Lett. **45**, 1196 (1980).

[13]M. Parrinello and A. Rahman, "Polymorphic transitions in single crystals: A new molecular dynamics method," J. Appl. Phys. **52**, 7182–7190 (1981).

[14]S. Nosé and M. L. Klein, "Structural transformations in solid nitrogen at high pressure," Phys. Rev. Lett. **50**, 1207 (1983).

[15]S. Nosé and M. L. Klein, "Constant pressure molecular dynamics for molecular systems," Mol. Phys. **50**, 1055–1076 (1983).

[16]S. Nosé and M. L. Klein, "A study of solid and liquid carbon tetrafluoride using the constant pressure molecular dynamics technique," J. Chem. Phys. **78**, 6928–6939 (1983).

[17]S. Nosé, "A molecular dynamics method for simulations in the canonical ensemble," Mol. Phys. **52**, 255–268 (1984).

[18]S. Nosé, "A unified formulation of the constant temperature molecular dynamics methods," J. Chem. Phys. **81**, 511–519 (1984).

[19]M. L. Klein, "Computer simulation studies of solids," Annu. Rev. Phys. Chem. **36**, 525–548 (1985).

[20]W. G. Hoover, "Canonical dynamics: Equilibrium phase-space distributions," Physi. Rev. A **31**, 1695 (1985).

[21]R. Car and M. Parrinello, "Unified approach for molecular dynamics and density-functional theory," Phys. Rev. Lett. **55**, 2471 (1985).

[22]G. Ciccotti and J.-P. Ryckaert, "Molecular dynamics simulation of rigid molecules," Comput. Phys. Rep. **4**, 346–392 (1986).

[23]K. Kremer and G. Grest, "Dynamics of entangled linear polymer melts: A molecular-dynamics simulation," J. Chem. Phys. **92**, 5057–5086 (1990).

[24]S. Nose, "Constant-temperature molecular dynamics," J. Phys.: Condens. Matter **2**, SA115 (1990).

[25]G. J. Martyna, M. L. Klein, and M. Tuckerman, "Nosé–Hoover chains: The canonical ensemble via continuous dynamics," J. Chem. Phys. **97**, 2635–2643 (1992).

[26]A. Laio and M. Parrinello, "Escaping free-energy minima," Proc. Natl. Acad. Sci. U. S. A. **99**, 12562–12566 (2002).

[27]G. Bussi, D. Donadio, and M. Parrinello, "Canonical sampling through velocity rescaling," J. Chem. Phys. **126**, 014101 (2007).

[28]J. Behler and M. Parrinello, "Generalized neural-network representation of high-dimensional potential-energy surfaces," Phys. Rev. Lett. **98**(14), 146401 (2007).

[29]A. P. Bartók, M. C. Payne, R. Kondor, and G. Csányi, "Gaussian approximation potentials: The accuracy of quantum mechanics, without the electrons," Phys. Rev. Lett. **104**, 136403 (2010).

[30]D. Lu, H. Wang, M. Chen, L. Lin, R. Car, W. E, W. Jia, and L. Zhang, "86 PFLOPS deep potential molecular dynamics simulation of 100 million atoms with *ab initio* accuracy," Comput. Phys. Commun. **259**, 107624 (2021).

[31]L. Zhang, H. Wang, R. Car, and W. E, "Phase diagram of a deep potential water model," Phys. Rev. Lett. **126**, 236001 (2021).

[32]L. Bonati, E. Trizio, A. Rizzi, and M. Parrinello, "A unified framework for machine learning collective variables for enhanced sampling simulations: mlcolvar," J. Chem. Phys. **159**, 014801 (2023).

[33]J. Zeng, D. Zhang, D. Lu, P. Mo, Z. Li, Y. Chen, M. Rynik, L. Huang, Z. Li, S. Shi *et al.*, "DeePMD-kit v2: A software package for deep potential models," J. Chem. Phys. **159**, 054801 (2023).

[34]A. M. Turing, "On computable numbers, with an application to the entscheidungsproblem," Proc. London Math. Soc. **s2-42**, 230 (1936).

[35]W. Aspray, "John von Neumann's contributions to computing and computer science," IEEE Ann. History Comput. **11**, 189–195 (1989).

[36]M. Levitt, "The birth of computational structural biology," Nat. Struct. Mol. Biol. **8**, 392 (2001).

[37]A. T. Hagler, E. Huler, and S. Lifson, "Energy functions for peptides and proteins. I. Derivation of a consistent force field including the hydrogen bond from amide crystals," J. Am. Chem. Soc. **96**, 5319–5327 (1974).

[38]T. Schlick, R. Collepardo-Guevara, L. A. Halvorsen, S. Jung, and X. Xiao, "Biomolecular modeling and simulation: A field coming of age," Q. Rev. Biophys. **44**, 191–228 (2011).

[39]T. Schlick, S. Portillo-Ledesma, C. G. Myers, L. Beljak, J. Chen, S. Dakhel, D. Darling, S. Ghosh, J. Hall, M. Jan, E. Liang, S. Saju, M. Vohr, C. Wu, Y. Xu, and E. Xue, "Biomolecular modeling and simulation: A prospering multidisciplinary field," Annu. Rev. Biophys. **50**, 267–301 (2021).

[40]J. Tersoff, "New empirical approach for the structure and energy of covalent systems," Phys. Rev. B **37**, 6991–7000 (1988).

[41]A. C. T. van Duin, S. Dasgupta, F. Lorant, and W. A. Goddard, "ReaxFF: A reactive force field for hydrocarbons," J. Phys. Chem. A **105**(41), 9396–9409 (2001).

[42]T. P. Senftle, S. Hong, M. M. Islam, S. B. Kylasa, Y. Zheng, Y. K. Shin, C. Junkermeier, R. Engel-Herbert, M. J. Janik, H. M. Aktulga, T. Verstraelen, A. Grama, and A. C. T. van Duin, "The ReaxFF reactive force-field: Development, applications and future directions," npj Comput. Mater. **2**, 15011 (2016).

[43]G. Fiorin, M. J. DelloStritto, S. Percec, and M. L. Klein, "Shear response in crystalline models of poly(p-phenylene terephthalamide)," Mol. Phys. **119**, e1948122 (2021).

[44]F. V. Prudente and J. J. Soares Neto, "The fitting of potential energy surfaces using neural networks. Application to the study of the photodissociation processes," Chem. Phys. Lett. **287**(5–6), 585–589 (1998).

[45]T. B. Blank, S. D. Brown, A. W. Calhoun, and D. J. Doren, "Neural network models of potential energy surfaces," J. Chem. Phys. **103**, 4129–4137 (1995).

[46]M. F. Calegari Andrade, H.-Y. Ko, L. Zhang, R. Car, and A. Selloni, "Free energy of proton transfer at the water–TiO_2 interface from *ab initio* deep potential molecular dynamics," Chem. Sci. **11**(9), 2335–2341 (2020).

[47]W. Jia, H. Wang, M. Chen, D. Lu, L. Lin, R. Car, E. Weinan, and L. Zhang, "Pushing the limit of molecular dynamics with ab initio accuracy to 100 million atoms with machine learning," in *SC20: International Conference for High Performance Computing, Networking, Storage and Analysis* (IEEE, 2020), pp. 1–14.
[48]S. Zhang, M. Z. Makoś, R. B. Jadrich, E. Kraka, K. Barros, B. T. Nebgen, S. Tretiak, O. Isayev, N. Lubbers, R. A. Messerly, and J. S. Smith, "Exploring the frontiers of condensed-phase chemistry with a general reactive machine learning potential," Nat. Chem. **16**, 727 (2024).
[49]D. Li, D. Zhao, Y. Huang, H. Shen, and M. Deng, "Modelling infrared spectra of the O-H stretches in liquid H_2O based on a deep learning potential, the importance of nuclear quantum effects," Mol. Simul. **50**, 539–546 (2024).
[50]X. Bian and J. E. Subotnik, "Angular momentum transfer between a molecular system and a continuous circularly polarized light field within a semiclassical Born–Oppenheimer surface hopping framework," J. Chem. Theory Comput. **20**, 6442–6453 (2024).
[51]C. Micheletti, D. Marenduzzo, E. Orlandini, and D. W. Summers, "Knotting of random ring polymers in confined spaces," J. Chem. Phys. **124**, 64903 (2006).
[52]P. G. de Gennes, "Reptation of a polymer chain in the presence of fixed obstacles," J. Chem. Phys. **55**, 572–579 (1971).
[53]R. Everaers, S. K. Sukumaran, G. S. Grest, C. Svaneborg, A. Sivasubramanian, and K. Kremer, "Rheology and microscopic topology of entangled polymeric liquids," Science **303**, 823–826 (2004).
[54]J. Tang, N. Du, and P. S. Doyle, "Compression and self-entanglement of single DNA molecules under uniform electric field," Proc. Natl. Acad. Sci. U. S. A. **108**, 16153–16158 (2011).
[55]M. Di Stefano, L. Tubiana, M. Di Ventra, and C. Micheletti, "Driving knots on DNA with AC/DC electric fields: Topological friction and memory effects," Soft Matter **10**, 6491–6498 (2014).
[56]S. Amin, A. Khorshid, L. Zeng, P. Zimny, and W. Reisner, "A nanofluidic knot factory based on compression of single DNA in nanochannels," Nat. Commun. **9**, 1506 (2018).
[57]D. Michieletto, E. Orlandini, M. S. Turner, and C. Micheletti, "Separation of geometrical and topological entanglement in confined polymers driven out of equilibrium," ACS Macro Lett. **9**, 1081–1085 (2020).
[58]V. Sorichetti, A. Ninarello, J. Ruiz-Franco, V. Hugouvieux, E. Zaccarelli, C. Micheletti, W. Kob, and L. Rovigatti, "Structure and elasticity of model disordered, polydisperse, and defect-free polymer networks," J. Chem. Phys. **158**, 074905 (2023).
[59]P. Giannozzi, S. Baroni, N. Bonini, M. Calandra, R. Car, C. Cavazzoni, D. Ceresoli, G. L. Chiarotti, M. Cococcioni, I. Dabo, A. Dal Corso, S. de Gironcoli, S. Fabris, G. Fratesi, R. Gebauer, U. Gerstmann, C. Gougoussis, A. Kokalj, M. Lazzeri, L. Martin-Samos, N. Marzari, F. Mauri, R. Mazzarello, S. Paolini, A. Pasquarello, L. Paulatto, C. Sbraccia, S. Scandolo, G. Sclauzero, A. P. Seitsonen, A. Smogunov, P. Umari, and R. M. Wentzcovitch, "QUANTUM ESPRESSO: A modular and open-source software project for quantum simulations of materials," J. Phys.: Condens. Matter **21**(39), 395502 (2009).
[60]P. Giannozzi, O. Andreussi, T. Brumme, O. Bunau, M. Buongiorno Nardelli, M. Calandra, R. Car, C. Cavazzoni, D. Ceresoli, M. Cococcioni, N. Colonna, I. Carnimeo, A. Dal Corso, S. de Gironcoli, P. Delugas, R. A. DiStasio, Jr, A. Ferretti, A. Floris, G. Fratesi, G. Fugallo, R. Gebauer, U. Gerstmann, F. Giustino, T. Gorni, J. Jia, M. Kawamura, H.-Y. Ko, A. Kokalj, E. Küçükbenli, M. Lazzeri, M. Marsili, N. Marzari, F. Mauri, N. L. Nguyen, H.-V. Nguyen, A. Otero-de-la-Roza, L. Paulatto, S. Poncé, D. Rocca, R. Sabatini, B. Santra, M. Schlipf, A. P. Seitsonen, A. Smogunov, I. Timrov, T. Thonhauser, P. Umari, N. Vast, X. Wu, and S. Baroni, "Advanced capabilities for materials modelling with QUANTUM ESPRESSO," J. Phys.: Condens. Matter **29**(46), 465901 (2017).
[61]J. W. Furness, A. D. Kaplan, J. Ning, J. P. Perdew, and J. Sun, "Accurate and numerically efficient r^2SCAN meta-generalized gradient approximation," J. Phys. Chem. Lett. **11**(19), 8208–8215 (2020).
[62]Y. Yao and Y. Kanai, "Plane-wave pseudopotential implementation and performance of SCAN meta-GGA exchange-correlation functional for extended systems," J. Chem. Phys. **146**(22), 224105 (2017).
[63]L. Martínez, R. Andrade, E. G. Birgin, and J. M. Martínez, "PACKMOL: A package for building initial configurations for molecular dynamics simulations," J. Comput. Chem. **30**(13), 2157–2164 (2009).
[64]J. Behler, "Constructing high-dimensional neural network potentials: A tutorial review," Int. J. Quantum Chem. **115**(16), 1032–1050 (2015).
[65]S. W. I. Siu, K. Pluhackova, and R. A. Böckmann, "Optimization of the OPLS-AA force field for long hydrocarbons," J. Chem. Theory Comput. **8**(4), 1459–1470 (2012).
[66]D. W. Sumners and S. G. Whittington, "Knots in self-avoiding walks," J. Phys. A: Math. Gen. **21**, 1689–1694 (1988).
[67]A. Dobay, J. Dubochet, K. Millett, P.-E. Sottas, and A. Stasiak, "Scaling behavior of random knots," Proc. Natl. Acad. Sci. U. S. A. **100**, 5611–5615 (2003).
[68]N. T. Moore, R. C. Lua, and A. Y. Grosberg, "Topologically driven swelling of a polymer loop," Proc. Natl. Acad. Sci. U. S. A. **101**, 13431–13435 (2004).
[69]S. A. Wasserman and N. R. Cozzarelli, "Biochemical topology: Applications to DNA recombination and replication," Science **232**, 951–960 (1986).
[70]A. Valdés, B. Martínez-García, J. Segura, S. Dyson, O. Díaz-Ingelmo, and J. Roca, "Quantitative disclosure of DNA knot chirality by high-resolution 2D-gel electrophoresis," Nucleic Acids Res. **47**, e29 (2019).
[71]B. Marcone, E. Orlandini, A. L. Stella, and F. Zonta, "What is the length of a knot in a polymer?," J. Phys. A: Math. Gen. **38**, L15 (2004).
[72]A. Y. Grosberg and Y. Rabin, "Metastable tight knots in a wormlike polymer," Phys. Rev. Lett. **99**, 217801 (2007).
[73]L. Tubiana, A. Rosa, F. Fragiacomo, and C. Micheletti, "Spontaneous knotting and unknotting of flexible linear polymers: Equilibrium and kinetic aspects," Macromolecules **46**, 3669–3678 (2013).
[74]L. Dai, C. B. Renner, and P. S. Doyle, "Metastable tight knots in semiflexible chains," Macromolecules **47**, 6135–6140 (2014).
[75]Y.-J. Sheng, P.-Y. Lai, and H.-K. Tsao, "Topological effects on statics and dynamics of knotted polymers," Phys. Rev. E **58**, R1222–R1225 (1998).
[76]R. Metzler, W. Reisner, R. Riehn, R. Austin, J. O. Tegenfeldt, and I. M. Sokolov, "Diffusion mechanisms of localised knots along a polymer," Europhys. Lett. **76**, 696 (2006).
[77]Z. Ma and K. D. Dorfman, "Diffusion of knots along DNA confined in nanochannels," Macromolecules **53**, 6461–6468 (2020).
[78]R. Mao and K. D. Dorfman, "Diffusion of knots in nanochannel-confined DNA molecules," J. Chem. Phys. **158**, 194901 (2023).
[79]J. P. J. Michels and F. W. Wiegel, "On the topology of a polymer ring," Proc. R. Soc. London, Ser. A **403**, 269–284 (1986).
[80]M. C. Tesi, E. J. Janse Van Rensburg, E. Orlandini, and S. G. Whittington, "Topological entanglement complexity of polymer chains in confined geometries," in *Topology and Geometry in Polymer Science*, *IMA Volumes in Mathematics and Its Application Vol. 103*, edited by S. G. Whittington, D. W. Sumners, and T. Lodge (Topology and Geometry in Polymer Science, 1998), pp. 135–157.
[81]J. Arsuaga, M. Vázquez, S. Trigueros, D. W. Sumners, and J. Roca, "Knotting probability of DNA molecules confined in restricted volumes: DNA knotting in phage capsids," Proc. Natl. Acad. Sci. U. S. A. **99**, 5373–5377 (2002).
[82]C. Micheletti and E. Orlandini, "Knotting and unknotting dynamics of DNA strands in nanochannels," ACS Macro Lett. **3**, 876–880 (2014).
[83]V. López, M.-L. Martínez-Robles, P. Hernández, D. B. Krimer, and J. B. Schvartzman, "Topo IV is the topoisomerase that knots and unknots sister duplexes during DNA replication," Nucleic Acids Res. **40**, 3563–3573 (2011).
[84]L. Postow, N. J. Crisona, B. J. Peter, C. D. Hardy, and N. R. Cozzarelli, "Topological challenges to DNA replication: Conformations at the fork," Proc. Natl. Acad. Sci. U. S. A. **98**, 8219–8226 (2001).
[85]R. W. Deibler, S. Rahmati, and E. L. Zechiedrich, "Topoisomerase IV, alone, unknots DNA in *E. coli*," Genes Dev. **15**, 748–761 (2001).
[86]K. Shishido, S. Ishii, and N. Komiyama, "The presence of the region on pBR322 that encodes resistance to tetracycline is responsible for high levels of plasmid DNA knotting in *Echerichia coli* DNA topoisomerase I deletion mutant," Nucleic Acids Res. **17**, 9749–9759 (1989).
[87]K. Shishido, N. Komiyama, and S. Ikawa, "Increased production of a knotted form of plasmid pBR322 DNA in *Escherichia coli* DNA topoisomerase mutants," J. Mol. Biol. **195**, 215–218 (1987).
[88]J. Portugal and A. Rodríguez-Campos, "T7 RNA polymerase cannot transcribe through a highly knotted DNA template," Nucleic Acids Res. **24**, 4890–4894 (1996).

[89]A. Valdés, L. Coronel, B. Martínez-García, J. Segura, S. Dyson, O. Díaz-Ingelmo, C. Micheletti, and J. Roca, "Transcriptional supercoiling boosts topoisomerase II-mediated knotting of intracellular DNA," Nucleic Acids Res. **47**, 6946–6955 (2019).
[90]C. Plesa, S. W. Kowalczyk, R. Zinsmeester, A. Y. Grosberg, Y. Rabin, and C. Dekker, "Fast translocation of proteins through solid state nanopores," Nano Lett. **13**, 658–663 (2013).
[91]C. Plesa, D. Verschueren, S. Pud, J. Van Der Torre, J. W. Ruitenberg, M. J. Witteveen, M. P. Jonsson, A. Y. Grosberg, Y. Rabin, and C. Dekker, "Direct observation of DNA knots using a solid-state nanopore," Nat. Nanotechnol. **11**, 1093–1097 (2016).
[92]P. Virnau, Y. Kantor, and M. Kardar, "Knots in globule and coil phases of a model polyethylene," J. Am. Chem. Soc. **127**, 15102–15106 (2005).
[93]E.-G. Kim and M. L. Klein, "Unknotting of a polymer strand in a melt," Macromolecules **37**, 1674–1677 (2004).
[94]F. Christakopoulos, E. Troisi, N. Friederichs, J. Vermant, and T. A. Tervoort, "'Tying the knot': Enhanced recycling through ultrafast entangling across ultra-high molecular weight polyethylene interfaces," Macromolecules **54**, 9452–9460 (2021).
[95]A. Rosa, M. Di Ventra, and C. Micheletti, "Topological jamming of spontaneously knotted polyelectrolyte chains driven through a nanopore," Phys. Rev. Lett. **109**, 118301 (2012).
[96]A. Suma, A. Rosa, and C. Micheletti, "Pore translocation of knotted polymer chains: How friction depends on knot complexity," ACS Macro Lett. **4**, 1420–1424 (2015).
[97]R. R. Wilcox, *Introduction to Robust Estimation and Hypothesis Testing* (Academic Press, 2012).
[98]E. Evans, "Probing the relation between force—lifetime—and chemistry in single molecular bonds," Annu. Rev. Biophys. Biomol. Struct. **30**, 105–128 (2001).
[99]O. K. Dudko, G. Hummer, and A. Szabo, "Theory, analysis, and interpretation of single-molecule force spectroscopy experiments," Proc. Natl. Acad. Sci. U. S. A. **105**, 15755–15760 (2008).
[100]O. Björnham and M. Andersson, "Theory for nonlinear dynamic force spectroscopy," Eur. Biophys. J. **46**, 225–233 (2017).
[101]X. Glorot, A. Bordes, and Y. Bengio, "Deep sparse rectifier neural networks," in *Proceedings of the Fourteenth International Conference on Artificial Intelligence and Statistics (JMLR Workshop and Conference Proceedings)* (Proceedings of Machine Learning Research, 2011), pp. 315–323.
[102]C. W. Ashley, *The Ashley Book of Knots*, 1st ed. (Doubleday, New York, 1993).
[103]A. M. Saitta, P. D. Soper, E. Wasserman, and M. L. Klein, "Influence of a knot on the strength of a polymer strand," Nature **399**, 46–48 (1999).
[104]A. M. Saitta and M. L. Klein, "Polyethylene under tensil load: Strain energy storage and breaking of linear and knotted alkanes probed by first-principles molecular dynamics calculations," J. Chem. Phys. **111**, 9434–9440 (1999).
[105]P. Pieranski, S. Kasas, G. Dietler, J. Dubochet, and A. Stasiak, "Localization of breakage points in knotted strings," New J. Phys. **3**, 10 (2001).
[106]A. M. Saitta and M. L. Klein, "First-principles molecular dynamics study of the rupture processes of a bulklike polyethylene knot," J. Phys. Chem. B **105**, 6495–6499 (2001).
[107]L. Tubiana, G. Polles, E. Orlandini, and C. Micheletti, "KymoKnot: A web server and software package to identify and locate knots in trajectories of linear or circular polymers," Eur. Phys. J. E **41**, 72 (2018).
[108]L. Tubiana, E. Orlandini, and C. Micheletti, "Probing the entanglement and locating knots in ring polymers: A comparative study of different arc closure schemes," Prog. Theor. Phys. Suppl. **191**, 192–204 (2011).
[109]M. DelloStritto and M. L. Klein, "Understanding strain and failure of a knot in polyethylene using molecular dynamics with machine-learned potentials," J. Phys. Chem. Lett. **15**, 9070–9077 (2024).